Bifurcations of a plane parallel flow with Kolmogorov forcing

Kannabiran Seshasayanan,[1,*] Vassilios Dallas,[2,†] and Stephan Fauve[3,‡]
[1]*Department of Physics, Indian Institute of Technology Kharagpur, Kharagpur 721 302, India*
[2]*Mathematical Institute, University of Oxford, Woodstock Road, Oxford OX2 6GG, United Kingdom*
[3]*Laboratoire de Physique de l'École normale supérieure, ENS, Université PSL, CNRS, Sorbonne Université, Université Paris-Diderot, Sorbonne Paris Cité, Paris F-75005, France*

(Received 26 April 2020; accepted 28 September 2021; published 14 October 2021)

We study the primary bifurcations of a two-dimensional Kolmogorov flow in a channel subject to boundary conditions chosen to mimic a parallel flow, i.e., periodic and free-slip boundary conditions in the streamwise and spanwise directions, respectively. The control parameter is the Reynolds number based on the friction coefficient, denoted as Rh. We find that as we increase Rh the laminar steady flow can display different types of bifurcation depending on the forcing wave number of the base flow. This is in contrast with the case of doubly periodic boundary conditions for which the primary bifurcation is stationary. In the present case, both stationary and Hopf bifurcations are observed. In addition, we discover a type of bifurcation with both the oscillation frequency and the amplitude of the growing mode being zero at the threshold, that we call a stationary drift bifurcation. A reduced four-mode model captures the scalings that are obtained from the numerical simulations. As we increase Rh further we observe a secondary instability which excites the largest mode in the domain. The saturated amplitude of the largest mode is found to scale as a $3/2$ power law of the distance to the threshold which is also explained using a low-dimensional model.

DOI: 10.1103/PhysRevFluids.6.103902

I. INTRODUCTION

The two-dimensional flow in a doubly periodic domain driven by a sine wave body forcing was first introduced in 1959 by Kolmogorov [1] as a mathematically tractable problem to study flow stability. It has been shown that this flow is unstable above a critical Reynolds number of order one in the limit of an unbounded flow domain [2]. The instability occurs at vanishing wave number which has been used to perform a weakly nonlinear analysis showing that a large-scale flow is generated through a stationary bifurcation [3–5].

Experiments on Kolmogorov flows were first carried out using thin layers of electrolytes [6] or liquid metals [7] with spatially periodic driving by the Lorentz force and more recently in soap films with hydrodynamic driving [8]. It was realized that in all realistic configurations, a linear friction force should be added to the two-dimensional Navier-Stokes equation in order to model the experimental results. In the case of a one-dimensional spatial forcing, this friction term inhibits the large-scale flow such that the first instability occurs at finite wave number.

Another important aspect concerns the effect of boundary conditions. Mixed boundary conditions have been used in order to mimic experimental configurations. Periodic boundary conditions have

*s.kannabiran@gmail.com
†vassilios.dallas@gmail.com
‡fauve@lps.ens.fr

been kept in the streamwise direction whereas stress-free boundary conditions have been used in the spanwise direction. This lateral confinement of the base flow suppresses the instability at vanishing wave number even in the absence of linear friction [9,10]. The instability comes in at finite wave number although the wave number decreases when the confinement length L is increased [10]. The first instability threshold decreases to the value of the unbounded flow in the $L \gg 1$ limit. More surprisingly, the nature of the primary bifurcation depends on the confinement. It has been first experimentally observed that in the case of strong confinement, when only half wave length of the base flow fits in the channel ($N = 1$), the first instability is oscillatory [11], whereas it is stationary for $N = 6$ [6]. It has been observed later that the nature of the bifurcation depends on the parity of N [12]. Traveling waves are generated when N is odd, whereas a stationary regime is observed when N is even except for $N = 4$ for which an oscillatory regime is found. Linear stability analysis confirmed that the value of N affects the nature of the bifurcation. A Hopf bifurcation occurs for $N = 2$, whereas it is stationary for $N = 4$ and $N = 6$ [9]. This is not in agreement with the experiments, but we note that the lateral boundary conditions are different. The nature of the bifurcation with respect to the flow confinement has been carefully analyzed [13–15], but no simple argument has been put forward. Note that the definition of N in [9] is based on the number of the wavelengths instead of the number of half wavelengths as defined here.

In this study we show that even though the growth rate of the first instability is real for $N = 4$, the bifurcation is not, strictly speaking, a stationary one because a limit cycle is generated above threshold. However, its frequency vanishes at the instability onset. This process does not belong to one of the generic bifurcation scenarios that generate a limit cycle. A supercritical Hopf bifurcation occurs at vanishing amplitude but finite frequency. In contrast, a limit cycle can be generated with finite amplitude and infinite period when two fixed points on an invariant cycle undergo a saddle-node bifurcation and disappear or when a limit cycle collides with a saddle point leading to a homoclinic bifurcation [16]. In our case, both the amplitude and the frequency of the limit cycle vanish at threshold. We understand this behavior using a reduced set of interacting triads in Sec. IV.

As recalled above, in the case of a one-dimensional forcing, fluid friction as well as lateral confinement of the flow prevent the generation of a large-scale flow at the primary instability threshold. However, in two-dimensional forcing configurations, it has been observed that a large-scale shear flow can be generated by the first instability of a linear array of confined counter-rotating vortices [17]. This has been confirmed by numerical simulations [18] but a weakly nonlinear analysis of the type [3,4] is not possible in that case due to the boundary conditions. Above the primary instability mentioned before, the flow becomes two-dimensional, and we could expect that a secondary bifurcation generates a large-scale flow. This indeed occurs and a streamwise-independent shear flow with half of a wave length fitting in the channel is generated. Its amplitude increases above threshold with a $3/2$ power-law scaling which is at odds with respect to the characteristic behavior of supercritical bifurcations. A $1/2$ power-law scaling is observed most of the time except in the vicinity of tricritical points for which the coefficient of cubic nonlinearities vanishes giving rise to a $1/4$ power-law scaling [19]. The $3/2$ power-law scaling results from the nonlinear forcing of the shear flow by modes that bifurcate at the secondary instability threshold. The large-scale shear flow breaks mirror symmetry with respect to the midplane of the channel such that two mean flow solutions with opposite signs exist. When a turbulent regime is reached, random mean flow reversals are observed, which were recently studied in [20].

The article is organized as follows. In Sec. II we describe the flow configuration. In Sec. III we present results about the first and the second bifurcations undergone by the system from direct numerical simulations (DNS) of the fully nonlinear system and from the eigenvalue problem of the linearised system. Next in Sec. IV we explain the results obtained from DNS with the help of reduced models of interacting modes. Conclusions are presented in Sec. V.

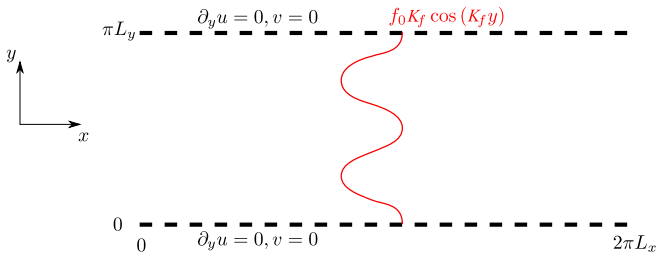

FIG. 1. Sketch of the domain under study. The red line represents the spatial form of the Kolmogorov forcing. Note that $f_0 K_f \cos(K_f y)$ profile corresponds to the force that acts on u, the x-component of the velocity field.

II. PROBLEM SETUP

We consider the two-dimensional Navier-Stokes equations for an incompressible velocity field $\mathbf{u} = \boldsymbol{\nabla} \times \Psi \hat{\mathbf{z}}$ forced by a Kolmogorov-type forcing in a domain of extent $(x, y) \in [0, 2\pi L_x] \times [0, \pi L_y]$ as illustrated in Fig. 1. The governing equation written in terms of the streamfunction $\Psi(x, y, t)$ is given by [4]

$$\partial_t \Psi + \boldsymbol{\nabla}^{-2}\{\boldsymbol{\nabla}^2 \Psi, \Psi\} = \nu \boldsymbol{\nabla}^2 \Psi - \mu \Psi + f_0 \sin(K_f y), \tag{1}$$

where $\{f, g\} = (\partial_x f)(\partial_y g) - (\partial_x g)(\partial_y f)$ is the standard Poisson bracket, ν is the kinematic viscosity, μ is the friction coefficient, f_0 is the amplitude of the Kolmogorov forcing and K_f is the forcing wave number. The boundary conditions are taken to be periodic in the x direction and free-slip in the y direction, i.e., $\Psi = \partial_y^2 \Psi = 0$ at $y = 0, \pi L_y$. Using L_x and $L_x / f_0^{1/2}$ as characteristic scales for space and time, respectively, we define the Reynolds number as $\mathrm{Re} = f_0^{1/2} L_x / \nu$ and the friction Reynolds number as

$$\mathrm{Rh} = f_0^{1/2} / (\mu L_x). \tag{2}$$

The dimensionless form of equation (1) for $\psi = \Psi / L_x f_0^{1/2}$ is

$$\partial_t \psi + \boldsymbol{\nabla}^{-2}\{\boldsymbol{\nabla}^2 \psi, \psi\} = \frac{1}{\mathrm{Re}} \boldsymbol{\nabla}^2 \psi - \frac{1}{\mathrm{Rh}} \psi + \sin(k_f y), \tag{3}$$

where $k_f = K_f L_x$ is the dimensionless forcing wave number and where we have kept the same notations for dimensionless space x, y and time t.

The control parameter of the problem is Rh and we fix the Reynolds number to $\mathrm{Re} = 1000$, the aspect ratio of the domain to $2\pi L_x / (\pi L_y) = 2$ (i.e., we set $L_x = L_y$) and the forcing wave number with respect to the height to $K_f L_y = k_f = 4$. The scaling behavior of the bifurcations we present in this article can be reproduced if one chooses the rms velocity as the relevant velocity scale instead of $f_0^{1/2}$. Our choice to nondimensionalize using $f_0^{1/2}$ makes the analytical calculations more convenient.

We perform direct numerical simulations (DNS) by integrating Eq. (1) using the pseudospectral method [21,22]. We decompose the streamfunction into basis functions with Fourier modes in the x direction and Sine modes in the y direction that satisfy the boundary conditions, this leads to

$$\psi(x, y, t) = \sum_{k_x = -\frac{N_x}{2}}^{\frac{N_x}{2} - 1} \sum_{k_y = 1}^{N_y} \widehat{\psi}_{k_x, k_y}(t)\, e^{i k_x x} \sin(k_y y), \tag{4}$$

with $\widehat{\psi}_{k_x, k_y}$ being the amplitude of the mode (k_x, k_y) and (N_x, N_y) denote the number of spectral modes in the x, y coordinates, respectively. For the streamfunction $\psi(x, y, t)$ to be real the following

TABLE I. The dependence of the nature of the first bifurcation on the forcing wave number k_f. The Reynolds number is fixed at Re = 1000 for all cases. The largest amplitude growing mode shown in the last column is found from the eigenvalue problem.

k_f	Linear problem	Nonlinearly saturated regime	Rh_1^c	Largest amplitude growing mode (k_x, k_y)
2	Hopf	Traveling wave	1.428	(1,1)
3	Hopf	Standing wave	1.077	(2,2)
4	Stationary	Traveling wave	0.593	(3,1)
5	Stationary	Stationary	0.446	(3,1)
6	Stationary	Traveling wave	0.352	(4,1)
7	Stationary	Stationary	0.299	(4,1)
8	Stationary	Traveling wave	0.256	(5,1)
9	Stationary	Stationary	0.227	(6,1)
10	Stationary	Traveling wave	0.202	(6,1)
63	Stationary	Stationary	0.0341	(36,1)
64	Stationary	Traveling wave	0.0336	(37,1)
127	Stationary	Stationary	0.0191	(72,1)
128	Stationary	Traveling wave	0.0190	(73,1)

relation is satisfied in spectral space

$$\widehat{\psi}_{k_x,k_y} = \widehat{\psi}^*_{-k_x,k_y}. \tag{5}$$

A third-order Runge-Kutta scheme is used for time advancement, and the aliasing errors are removed with the two-thirds dealiasing rule which implies that the maximum wave numbers are $k_x^{max} = N_x/3$ and $k_y^{max} = 2N_y/3$. The resolution was fixed to $(N_x, N_y) = (512, 128)$ for all the simulations done in this study. The only simulations that required 512^2 resolution were those with $k_f \geqslant 63$ (see Table I).

III. PRIMARY AND SECONDARY BIFURCATIONS

For small values of Rh a laminar flow is established which results from the balance between the forcing and the dissipation. Its expression is given by

$$\psi(x, y, t) = \frac{1}{16\mathrm{Re}^{-1} + \mathrm{Rh}^{-1}} \sin(4y). \tag{6}$$

This base flow corresponds to a parallel flow with the same spanwise structure as the forcing. We can represent the base flow in the Fourier-sine basis (4), which gives the only nonzero mode to be $\widehat{\psi}_{0,4} = 1/(16\mathrm{Re}^{-1} + \mathrm{Rh}^{-1})$. From the DNS we observe that this laminar flow becomes linearly unstable above the critical value of $\mathrm{Rh} > \mathrm{Rh}_1^c \approx 0.593$, with the instability breaking the translational invariance in the x direction. In Fig. 2(a) we show the time series from the DNS of the most dominant Fourier-sine mode $\widehat{\psi}_{3,1}(t)$ related to the instability, for different values of Rh above the threshold. The time series demonstrate that as we approach the threshold $\mathrm{Rh} - \mathrm{Rh}_1^c \ll 1$, both the amplitude and the oscillation frequency decrease. In Fig. 2(b) we show the standard deviation $\sigma(\widehat{\psi}_{3,1})$ and the oscillation frequency ω_f of the saturated mode $\widehat{\psi}_{3,1}$ as a function of the distance to the threshold $\mathrm{Rh} - \mathrm{Rh}_1^c$. To capture the exact threshold we linearize around the base flow solution (6), and we numerically solve the eigenvalue problem that arises from the linearized system of equations. The eigenvalue solver confirms the value of the threshold $\mathrm{Rh}_1^c \approx 0.593$ found from the DNS. The growing eigenmode has a wave number $k_x = 3$ in the x direction, and its projection on to sine basis in the y direction shows that only the odd modes $k_y = 2n + 1$, $n \in \mathbb{N}$ are excited. In addition, it shows that the eigenvalues are real therefore leading to either an exponentially growing

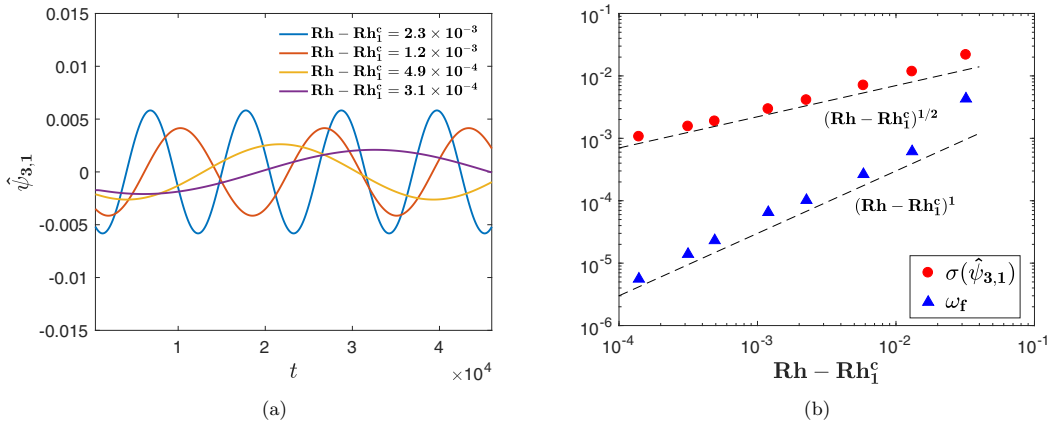

FIG. 2. (a) Time series of the growing mode $\widehat{\psi}_{3,1}$ for different values of Rh close to the threshold. (b) The standard deviation $\sigma(\widehat{\psi}_{3,1})$ and the oscillation frequency ω_f of the mode $\widehat{\psi}_{3,1}$ as a function of the distance to the threshold. The solution corresponds to a traveling wave that moves in the negative x-direction.

or decaying solution without any oscillatory behavior. This is in agreement with the linear stability analysis of Thess [9]. Therefore, the oscillations we observe result from the fully nonlinear problem, which is also responsible for the scaling of the frequency $\omega_f \propto \mathrm{Rh} - \mathrm{Rh}_1^c$. We call this transition a stationary drift bifurcation. The resulting solution from the nonlinear problem corresponds to a traveling wave that moves in the negative x-direction. A four-mode model is presented in Sec. IV B to explain the observed behavior.

We study the nature of the first bifurcation by varying k_f systematically, looking at both the linearized system and the fully nonlinear system. We note that k_f is nondimensional and changing k_f is equivalent to changing $K_f L_x$ in dimensional units. In Table I we report the results we get from the eigenvalue problem for the linearized system and from the DNS. For $k_f = 2, 3$ the linear problem gives rise to a Hopf bifurcation and the nonlinear regime is either a traveling or a standing wave. Then for $k_f \geqslant 4$ the linear problem gives rise to a stationary bifurcation, while the nonlinear problem gives a stationary pattern only when k_f is odd and a traveling pattern when k_f is even. These results with odd behavior do not allow us to have a general argument for the nature of the bifurcation for any k_f. On the other hand, we notice that even for the spatially extended system with $k_f \gg 1$ the mode $k_y = 1$ is always excited. Note, however, that the largest amplitude growing mode for $k_f = 3$ is not the one with $k_y = 1$, and this differs from the other cases. The case $k_f = 3$ is also the only odd forcing case that gives a Hopf bifurcation; see Table I.

It is commonly believed that the influence of the side walls on the instability should decrease when k_f becomes large such that the behavior predicted for unbounded Kolmogorov flows [9] should be recovered, i.e., a stationary pattern. This is not the case. The side walls, however distant, affect the nature of the bifurcation depending on the odd (respectively even) number of half-wavelengths of the base flow in the channel. This behavior traces back to the large-scale flow with $k_y = 1$ that is generated at the instability onset even for k_f large. A similar mechanism where distant side walls affect the nature of a bifurcation, has been described in the context of thermal convection [23]. Now we return to the case of $k_f = 4$ where the oscillating flow obtained for $\mathrm{Rh} > \mathrm{Rh}_1^c \approx 0.593$ persists up to $\mathrm{Rh} = \mathrm{Rh}_2^c \approx 0.835$, above which a Hopf bifurcation takes place and the largest scale mode of the system $\widehat{\psi}_{0,1}$ is excited. Figure 3 shows the x and the y components of the velocity field at two different time instants for $\mathrm{Rh} \approx 0.91$. The snapshots of the y component of the velocity field [Figs. 3(b) and 3(d)] show a modulated traveling wave moving along the negative x direction, the traveling wave corresponds to the flow obtained from the first bifurcation. The secondary instability then occurs on top of this traveling wave which makes the

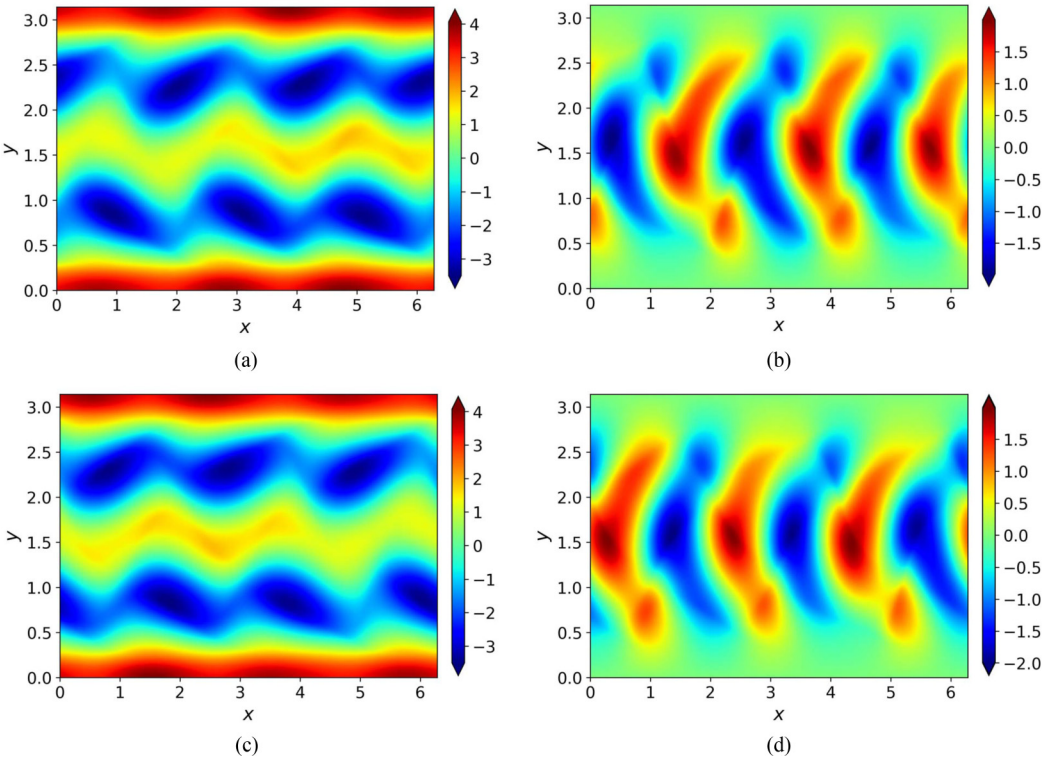

FIG. 3. Snapshots of the x-component (a, c) and y-components of the velocity fields (b, d) are shown at two different time instances for the case $\mathrm{Rh} \approx 0.91$. The solution corresponds to a modulated traveling wave that moves in the negative x-direction.

underlying wave modulated. This is similar to instabilities observed on wavy Taylor vortices in circular-Couette experiments (see [24,25]) with the resulting flow called modulated wavy-vortex flow. We believe that there is no frequency locking between the modulation frequency and the frequency of the traveling wave, similar to the case of circular-Couette experiments, though a much detailed analysis is required to show the absence of frequency locking. Figure 4 shows the standard deviation of $\widehat{\psi}_{0,1}$, denoted by $\sigma(\widehat{\psi}_{0,1})$, as a function of the distance to the threshold $\mathrm{Rh} - \mathrm{Rh}_2^c$ found from the DNS. The scaling we observe is $\sigma(\widehat{\psi}_{0,1}) \propto (\mathrm{Rh} - \mathrm{Rh}_2^c)^{3/2}$. This is distinctively different from the standard $1/2$ power-law scaling one expects for the saturated amplitude of the growing mode in the case of a supercritical Hopf bifurcation. This scaling results from the nonlinear excitation of the $\widehat{\psi}_{0,1}$ mode by the growing modes that bifurcate at $\mathrm{Rh} = \mathrm{Rh}_2^c$. A low-dimensional model is presented in Sec. IV C to explain this behavior.

IV. LOW-DIMENSIONAL DYNAMICAL SYSTEMS

A. Symmetry considerations

Before presenting a truncated model that explains our observations for $k_f = 4$, we first comment on the effect of the lateral confinement of the flow on the nature of the primary bifurcation using symmetry arguments. We write $\psi(x, y, t) = \psi_f(y) + \phi(x, y, t)$ where $\psi_f(y)$ is the base flow forced at wave number k_f. Equation (3) gives

$$\partial_t \nabla^2 \phi + \partial_y \psi_f \, \partial_x \left(\nabla^2 \phi + k_f^2 \phi \right) + \{ \nabla^2 \phi, \phi \} = \frac{1}{\mathrm{Re}} \nabla^4 \phi - \frac{1}{\mathrm{Rh}} \nabla^2 \phi. \tag{7}$$

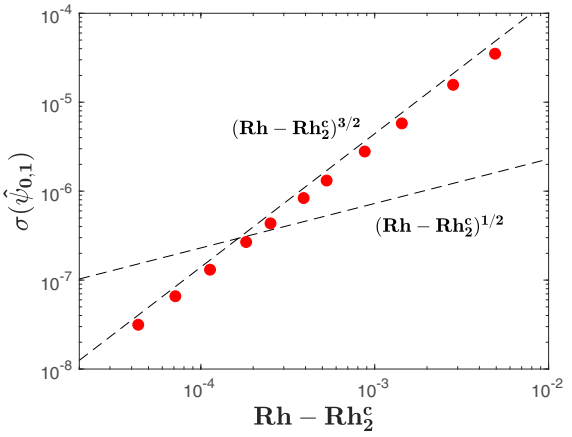

FIG. 4. The standard deviation of the largest scale mode $\widehat{\psi}_{0,1}$ as a function of the distance to the threshold $\mathrm{Rh}-\mathrm{Rh}_2^c$. The dashed lines indicate the scalings $(\mathrm{Rh}-\mathrm{Rh}_2^c)^{3/2}$ and $(\mathrm{Rh}-\mathrm{Rh}_2^c)^{1/2}$ for comparison.

In the case of doubly periodic boundary conditions, Eq. (7) is symmetric under the following transformations:

$$x \to x + x_0, \tag{8}$$

$$(x, y) \to \left(-x, -y + \frac{\pi}{k_f}\right), \tag{9}$$

$$(y, \psi_f, \phi) \to (-y, -\psi_f, -\phi), \tag{10}$$

$$y \to y + \frac{2\pi}{k_f}. \tag{11}$$

Equations (8) and (9) generate the $O(2)$ symmetry group, and the first bifurcation of the Kolmogorov flow $\psi_f(y)$ is either a stationary bifurcation with two zero eigenvalues or a Hopf bifurcation that leads to traveling or standing waves depending on the nonlinear interactions [26]. However, in the case of doubly periodic boundary conditions, the bifurcation that occurs first is always stationary [9]. Equation (10) involves the field ψ itself and is related to the pseudoscalar nature of Eq. (7) [27].

In the case of stress-free boundary conditions considered here, the shift π/k_f along the y-axis is no longer possible. Although it has been shown that these Neumann boundary conditions admit hidden symmetries that should be taken into account [28,29], it is clear from the results of Table I that the bifurcation picture with stress-free boundary conditions strongly differs from the one with doubly periodic boundary conditions. A Hopf bifurcation is observed for $k_f = 2$ and 3 whereas a stationary bifurcation occurs for $k_f \geqslant 4$. In addition, even in the case of a stationary bifurcation, stress-free boundary conditions display a puzzling result: the nonlinearly saturated regime above the bifurcation threshold is a traveling wave for k_f even, whereas it is stationary for k_f odd. Although general symmetry arguments cannot predict whether the linear problem is a stationary or a Hopf bifurcation, they can be used to understand the nature of the nonlinearly saturated regime for $k_f \geqslant 4$ as follows.

For $k_f \geqslant 4$, the bifurcation is stationary such that the perturbation that grows above threshold is to leading order of the form

$$\widetilde{\psi}(x, y, t) = A(t)\chi(y)\exp ik_c x + \text{c.c.}, \tag{12}$$

where A is the complex amplitude of the neutral mode of wave number k_c, $\chi(y)$ represents its dependence on y and "c.c." stands for the complex conjugate. Following [30] we expand $\dot{A}$ as a power series in A and A^* and we consider symmetry (8) to constrain the form of the amplitude equation to

$$\dot{A} = \alpha A - \beta A^2 A^*, \tag{13}$$

where α is real since the bifurcation is stationary and the asterisk denotes the complex conjugate. Note however that $\beta = \beta_r + i\beta_i$ is forced to be real only when another symmetry, usually related to the reflection symmetry $x \to -x$, imposes the invariance $A \to \pm A^*$ of the amplitude equation. This is the case for doubly periodic boundary conditions because of Eqs. (8) and (9) and the postbifurcation regime is stationary as observed in the case of doubly periodic boundary conditions [3–5]. When there exists a preferred direction, β can be complex. For a supercritical bifurcation ($\beta_r > 0$), the squared modulus of the amplitude is given by $AA^* = \alpha_r/\beta_r$ and its phase is $\theta = -(\alpha_r\beta_i/\beta_r)t$. Therefore, the pattern (12) travels at constant velocity which gives a limit cycle frequency proportional to the distance to the threshold, as observed in our simulations. This stationary drift bifurcation where a stationary instability generates a traveling wave in the nonlinear regime has been described by adding nonlinear terms which breaks the $x \to -x$ symmetry to the Swift-Hohenberg equation [30]. This is however an *ad hoc* model whereas the phenomenon is reported here is a fluid dynamical problem without selecting linear and nonlinear terms with different symmetries in the governing equation.

We will now explain why different nonlinear regimes are observed with stress-free boundary conditions in the case of a stationary bifurcation, depending on k_f odd or even. The base flow described by $\psi_f(y)$ is changed in the transformation $x \to -x$ for both k_f odd or even, but for k_f odd, it is possible to compensate this change by performing the transformation $y \to \pi - y$ whereas this is not possible for k_f even because the base flow has mirror symmetry with respect to the midplane of the channel $y = \pi/2$. Therefore, if k_f is odd, the problem is invariant under the transformation

$$(x, y) \to (-x, \pi - y). \tag{14}$$

In addition, for all odd values of $k_f > 4$ that we have explored, we find that $\chi(y)$ of the neutral mode has a real part that is symmetric about the midline ($y = \pi/2$) and an imaginary part that is antisymmetric about the midline. Therefore we have $\chi(y) \to \chi^*(y)$ in the transformation $y \to \pi - y$. Applying the symmetry (14) amounts to $A \to A^*$ in Eq. (13), which enforces $\beta_i = 0$. Therefore, for k_f odd, the pattern above the bifurcation threshold is stationary.

For the problem under study which is the case of $k_f = 4$, the perturbation form given in Eq. (12) satisfies the symmetries given in Eqs. (8), (10), and (11). It is found that the bifurcation is stationary meaning α coefficient in the amplitude equation [Eq. (13)] is real. Whereas the coefficient of the nonlinear term β is complex leading to a traveling wave with a preferred direction. Thus the linear eigenvalue problem leads to a stationary bifurcation while the nonlinear problem gives rise to a traveling wave with a preferred direction.

B. Four-mode model for the stationary drift bifurcation

Now we present a four-mode model to get a better qualitative understanding of the bifurcation for the case $k_f = 4$, i.e., a stationary bifurcation as shown by solving the linear problem, but that generates traveling waves in the post-bifurcation nonlinearly saturated regime. To derive the governing equations we consider the Navier-Stokes equation in the Fourier-Sine basis form by substituting Eq. (4) into Eq. (1) to obtain

$$d_t \widehat{\psi}_{\mathbf{k}} = \sum_{\mathbf{p},\mathbf{q}} A_{\mathbf{k},\mathbf{p},\mathbf{q}} \widehat{\psi}_{\mathbf{p}} \widehat{\psi}_{\mathbf{q}} - (\mathrm{Re}^{-1}k^2 + \mathrm{Rh}^{-1})\widehat{\psi}_{\mathbf{k}} + f_0 \delta_{k_x,0}\, \delta_{k_y,4} \tag{15}$$

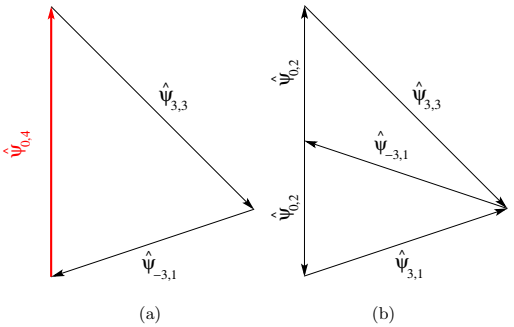

FIG. 5. All the interacting triads in the reduced four-mode model. In panel (b) the mode $\widehat{\psi}_{\mathbf{r}} = \widehat{\psi}_{0,2}$ is repeated twice as it is excited by the modes $\widehat{\psi}^*_{\mathbf{p}} = \widehat{\psi}_{-3,1}$, $\widehat{\psi}^*_{\mathbf{q}} = \widehat{\psi}_{3,3}$ and is also responsible for the oscillation of the mode $\widehat{\psi}_{3,1}$. The red arrow indicates the base flow mode $\widehat{\psi}_{0,4}$, which becomes unstable at the first threshold Rh_1^c.

with the interaction coefficients to be given by

$$A_{\mathbf{k},\mathbf{p},\mathbf{q}} = \frac{i}{2}(q^2 - p^2)k^{-2}\delta_{k_x,p_x+q_x}[(p_x q_y - p_y q_x)\delta_{k_y,p_y+q_y} + (p_x q_y + p_y q_x)(\delta_{k_y,p_y-q_y} - \delta_{k_y,q_y-p_y})], \tag{16}$$

where $\delta_{i,j}$ stands for the Kronecker delta and the variables p_x, p_y, q_x, q_y are the components of the wave vectors $\mathbf{p}$, $\mathbf{q}$, i.e., $\mathbf{p} = (p_x, p_y)$, $\mathbf{q} = (q_x, q_y)$. Consider a model with the base flow $\widehat{\psi}_{0,4}$, the two largest amplitude growing modes $\widehat{\psi}_{3,1}$, $\widehat{\psi}_{-3,3}$ and a nonlinear mode $\widehat{\psi}_{0,2}$, excited by the two growing modes. They are denoted as

$$\widehat{\psi}_{\mathbf{k}} = \widehat{\psi}_{0,4}, \quad \widehat{\psi}_{\mathbf{p}} = \widehat{\psi}_{3,1}, \quad \widehat{\psi}_{\mathbf{q}} = \widehat{\psi}_{-3,3}, \quad \widehat{\psi}_{\mathbf{r}} = \widehat{\psi}_{0,2}. \tag{17}$$

Using Eqs. (15) and (16), we arrive at the following system of equations:

$$d_t\widehat{\psi}_{\mathbf{k}} + (16\mathrm{Re}^{-1} + \mathrm{Rh}^{-1})\widehat{\psi}_{\mathbf{k}} = -3i(\widehat{\psi}^*_{\mathbf{p}}\widehat{\psi}^*_{\mathbf{q}} - \widehat{\psi}_{\mathbf{p}}\widehat{\psi}_{\mathbf{q}}) + 1, \tag{18}$$

$$d_t\widehat{\psi}_{\mathbf{p}} + (10\mathrm{Re}^{-1} + \mathrm{Rh}^{-1})\widehat{\psi}_{\mathbf{p}} = \frac{6}{5}i\widehat{\psi}_{\mathbf{k}}\widehat{\psi}^*_{\mathbf{q}} - \frac{21}{5}i\widehat{\psi}_{\mathbf{r}}\widehat{\psi}^*_{\mathbf{q}} - \frac{9}{5}i\widehat{\psi}_{\mathbf{p}}\widehat{\psi}_{\mathbf{r}}, \tag{19}$$

$$d_t\widehat{\psi}_{\mathbf{q}} + (18\mathrm{Re}^{-1} + \mathrm{Rh}^{-1})\widehat{\psi}_{\mathbf{q}} = 2i\widehat{\psi}_{\mathbf{k}}\widehat{\psi}^*_{\mathbf{p}} + i\widehat{\psi}_{\mathbf{r}}\widehat{\psi}^*_{\mathbf{p}}, \tag{20}$$

$$d_t\widehat{\psi}_{\mathbf{r}} + (4\mathrm{Re}^{-1} + \mathrm{Rh}^{-1})\widehat{\psi}_{\mathbf{r}} = 6i(\widehat{\psi}^*_{\mathbf{p}}\widehat{\psi}^*_{\mathbf{q}} - \widehat{\psi}_{\mathbf{p}}\widehat{\psi}_{\mathbf{q}}). \tag{21}$$

The triads that can be constructed from this set of modes are shown in Fig. 5, and we will discuss their dynamics in what follows. Here the constant term on the right of Eq. (18) is the forcing term which acts only on the mode $\widehat{\psi}_{\mathbf{k}}$. The base flow is given by the balance between the forcing and the dissipation in (18), which gives $\widehat{\psi}_{\mathbf{k}} = \psi_0 = 1/(16\mathrm{Re}^{-1} + \mathrm{Rh}^{-1})$. The instability is found by linearizing the above set of equations around the base flow ψ_0. In the linearized system, we see that only $\widehat{\psi}_{\mathbf{p}}$, $\widehat{\psi}_{\mathbf{q}}$ are coupled and the mode $\widehat{\psi}_{\mathbf{r}}$ is not coupled to the base flow. Then, the effective linearized system can be written as

$$d_t\widehat{\psi}_{\mathbf{p}} + (10\mathrm{Re}^{-1} + \mathrm{Rh}^{-1})\widehat{\psi}_{\mathbf{p}} = \frac{12i}{10}\psi_0\widehat{\psi}^*_{\mathbf{q}}, \tag{22}$$

$$d_t\widehat{\psi}^*_{\mathbf{q}} + (18\mathrm{Re}^{-1} + \mathrm{Rh}^{-1})\widehat{\psi}^*_{\mathbf{q}} = -2i\psi_0\widehat{\psi}_{\mathbf{p}}. \tag{23}$$

The linear stability threshold is found to be at $\mathrm{Rh}_1^c \approx 0.814$ and the Jacobian of Eqs. (22) and (23) gives two eigenmodes. Both eigenvalues are purely real leading to exponential growth or decay with no oscillations. We denote the amplitudes of the decaying and the growing eigenmode as $P_1(t)$ and

$P_2(t)$, respectively. The positive eigenvalue λ_2 that corresponds to the growing eigenmode P_2, scales linearly with the distance to the threshold

$$\lambda_2 \propto \left(\mathrm{Rh} - \mathrm{Rh}_1^c\right). \tag{24}$$

This scaling is true only close to the threshold. Its exact expression is given in the Appendix.

Now we choose to solve the nonlinear model with only the linearly excited modes, i.e., we consider only the triad $(\widehat{\psi}_{\mathbf{k}}, \widehat{\psi}_{\mathbf{p}}, \widehat{\psi}_{\mathbf{q}})$ given by Eqs. (18), (19), and (20) [see Fig. 5(a)] and with $\widehat{\psi}_{\mathbf{r}} = 0$. The modes $\widehat{\psi}_{\mathbf{p}}$, $\widehat{\psi}_{\mathbf{q}}$ are linearly excited by the instability of the base flow and saturate by modifying the amplitude of the mode $\widehat{\psi}_{\mathbf{k}}$. We then solve the full system of Eqs. (18)–(20) by focusing on the evolution of the growing eigenmode P_2. The resulting amplitude equation is

$$d_t P_2 = \lambda_2 P_2 - \left(\frac{\frac{36}{5}\zeta_2\beta_1 + 12\zeta_2^2\beta_3}{16\mathrm{Re}^{-1} + \mathrm{Rh}^{-1}}\right)|P_2|^2 P_2. \tag{25}$$

Details for its derivation and the expressions of the real coefficients $\zeta_2, \beta_1, \beta_3$ can be found in the Appendix. Thus, the amplitude equation for the three mode model $\widehat{\psi}_{\mathbf{k}}$, $\widehat{\psi}_{\mathbf{p}}$, $\widehat{\psi}_{\mathbf{q}}$ clearly gives rise to a stationary bifurcation with the scaling of the amplitude of the growing mode to be $|P_2| \propto (\mathrm{Rh} - \mathrm{Rh}_c)^{1/2}$ obtained from Eq. (24).

If we now consider Eq. (21), we see that the mode $\widehat{\psi}_{\mathbf{r}}$ is nonlinearly excited by the modes $\widehat{\psi}_{\mathbf{p}}$, $\widehat{\psi}_{\mathbf{q}}$ [see Fig. 5(b)]. This nonlinear excitation arises due to the transfer of energy from modes (p_x, p_y), (q_x, q_y) to both $(-p_x - q_x, p_y + q_y)$ and $(-p_x - q_x, |p_y - q_y|)$ in the Fourier-sine basis. Taking into account all the four modes we can get to the following amplitude equation:

$$\begin{aligned} d_t P_2 = \lambda_2 P_2 &- \left[\left(\frac{\frac{36}{5}\zeta_2\beta_1 + 12\zeta_2^2\beta_3}{16\mathrm{Re}^{-1} + \mathrm{Rh}^{-1}}\right) + \left(\frac{\frac{252}{5}\zeta_2\beta_1 - 12\zeta_2^2\beta_3}{4\mathrm{Re}^{-1} + \mathrm{Rh}^{-1}}\right)\right]|P_2|^2 P_2 \\ &- i\left(\frac{108}{5}\frac{\zeta_2^2\beta_1}{4\mathrm{Re}^{-1} + \mathrm{Rh}^{-1}}\right)|P_2|^2 P_2, \end{aligned} \tag{26}$$

where the expressions for $\lambda_2, \beta_1, \beta_3, \zeta_2$ are given in the Appendix. This amplitude equation is very similar to Eq. (25), the amplitude equation for the three-mode model, except for the presence of the complex coefficient in the final term which arises from the existence of $\widehat{\psi}_{\mathbf{r}}$. This term leads to oscillatory solutions of the form $P_2(t) = |P_2| \exp(i\omega_f t)$. By substituting this solution into Eq. (26) we get

$$|P_2|^2 = \lambda_2\left[\left(\frac{\frac{36}{5}\zeta_2\beta_1 + 12\zeta_2^2\beta_3}{16\mathrm{Re}^{-1} + \mathrm{Rh}^{-1}}\right) + \left(\frac{\frac{252}{5}\zeta_2\beta_1 - 12\zeta_2^2\beta_3}{4\mathrm{Re}^{-1} + \mathrm{Rh}^{-1}}\right)\right]^{-1}, \tag{27}$$

$$\omega_f = -\frac{108}{5}\frac{\zeta_2^2\beta_1}{4\mathrm{Re}^{-1} + \mathrm{Rh}^{-1}}|P_2|^2. \tag{28}$$

Using Eq. (24) we find the amplitude to scale similar to the three mode model, i.e., $|P_2| \propto (\mathrm{Rh} - \mathrm{Rh}_c)^{1/2}$ and the oscillation frequency to scale linearly with the distance to the threshold $\omega_f \propto (\mathrm{Rh} - \mathrm{Rh}_c)$. Thus, the minimal four-mode model reproduces the stationary drift bifurcation and the observed scalings of the DNS results. The value we obtain for the threshold does not agree quantitatively with the DNS. This is because in the DNS many modes are nonzero in contrast to our minimal model which considers only the four modes with the largest amplitude in the full system. By adding more modes and following the method presented above we can approach the values of the threshold and the oscillation frequency obtained in the DNS.

C. Large-scale bifurcation model

Here we present a model to explain the exponent 3/2 for the largest scale mode in the system $\widehat{\psi}_{0,1}$. This mode is directly excited by the nonlinear perturbations that grow after the second Hopf bifurcation. We present here a model with eight modes that is sufficient to capture the different

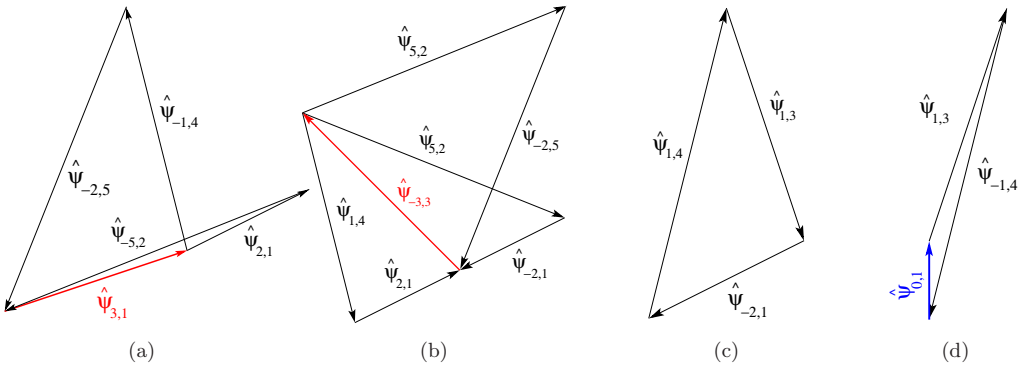

FIG. 6. All the interacting triads of the reduced eight-mode model. The red arrows indicate the modes that become unstable at the second threshold Rh_2^c, and the blue arrow indicates the large-scale mode $\widehat{\psi}_{0,1}$.

scalings needed to explain the exponent 3/2. The base flow over which the second instability develops involves multiple modes. We construct a reduced model using the following set of modes:

$$\begin{aligned}&\widehat{\psi}_{\mathbf{a}} = \widehat{\psi}_{-3,1}, \quad \widehat{\psi}_{\mathbf{b}} = \widehat{\psi}_{-3,3}, \quad \widehat{\psi}_{\mathbf{c}} = \widehat{\psi}_{1,4}, \quad \widehat{\psi}_{\mathbf{d}} = \widehat{\psi}_{2,5},\\ &\widehat{\psi}_{\mathbf{e}} = \widehat{\psi}_{2,1}, \quad \widehat{\psi}_{\mathbf{f}} = \widehat{\psi}_{-5,2}, \quad \widehat{\psi}_{\mathbf{g}} = \widehat{\psi}_{-1,3}, \quad \widehat{\psi}_{\mathbf{h}} = \widehat{\psi}_{0,1}.\end{aligned} \tag{29}$$

These modes are chosen because they have the largest amplitudes in the DNS. Moreover, we tested that if any of the modes are put to zero, then $\widehat{\psi}_{0,1}$ is not excited or it has a much lower amplitude. This demonstrates how vital these modes are to the excitation of the large-scale mode. Below the second instability all the aforementioned modes have zero amplitude apart from the modes $\widehat{\psi}_{\mathbf{a}} = \widehat{\psi}_{-3,1}$, $\widehat{\psi}_{\mathbf{b}} = \widehat{\psi}_{-3,3}$, which are already excited at the first instability. Above the threshold value of Rh_2^c, the modes $\widehat{\psi}_{\mathbf{a}} = \widehat{\psi}_{-3,1}$, $\widehat{\psi}_{\mathbf{b}} = \widehat{\psi}_{-3,3}$ become linearly unstable and give rise to the modes $\widehat{\psi}_{\mathbf{c}}$, $\widehat{\psi}_{\mathbf{d}}$, $\widehat{\psi}_{\mathbf{e}}$, $\widehat{\psi}_{\mathbf{f}}$. The triadic interactions are shown in Figs. 6(a) and 6(b). The governing equations for the unstable modes $\widehat{\psi}_{\mathbf{a}}$, $\widehat{\psi}_{\mathbf{b}}$ and the linearly excited modes $\widehat{\psi}_{\mathbf{c}}$, $\widehat{\psi}_{\mathbf{d}}$, $\widehat{\psi}_{\mathbf{e}}$, $\widehat{\psi}_{\mathbf{f}}$ are

$$d_t\widehat{\psi}_{\mathbf{a}} + (10\mathrm{Re}^{-1} + \mathrm{Rh}^{-1})\widehat{\psi}_{\mathbf{a}} = i\frac{39}{5}\widehat{\psi}_{\mathbf{c}}^*\widehat{\psi}_{\mathbf{d}}^* + i\frac{6}{5}\widehat{\psi}_{\mathbf{e}}\widehat{\psi}_{\mathbf{f}} + f_1, \tag{30}$$

$$d_t\widehat{\psi}_{\mathbf{b}} + (18\mathrm{Re}^{-1} + \mathrm{Rh}^{-1})\widehat{\psi}_{\mathbf{b}} = 3i\widehat{\psi}_{\mathbf{c}}^*\widehat{\psi}_{\mathbf{e}}^* + 6i\widehat{\psi}_{\mathbf{e}}\widehat{\psi}_{\mathbf{f}} + f_2, \tag{31}$$

$$d_t\widehat{\psi}_{\mathbf{c}} + \left(17\mathrm{Re}^{-1} + \mathrm{Rh}^{-1}\right)\widehat{\psi}_{\mathbf{c}} = -i\frac{247}{34}\widehat{\psi}_{\mathbf{d}}^*\widehat{\psi}_{\mathbf{a}}^* - i\frac{117}{34}\widehat{\psi}_{\mathbf{e}}^*\widehat{\psi}_{\mathbf{b}}^* + i\frac{35}{34}\widehat{\psi}_{\mathbf{e}}\widehat{\psi}_{\mathbf{g}} - i\frac{9}{34}\widehat{\psi}_{\mathbf{g}}^*\widehat{\psi}_{\mathbf{h}}, \tag{32}$$

$$d_t\widehat{\psi}_{\mathbf{d}} + \left(29\mathrm{Re}^{-1} + \mathrm{Rh}^{-1}\right)\widehat{\psi}_{\mathbf{d}} = i\frac{91}{58}\widehat{\psi}_{\mathbf{c}}^*\widehat{\psi}_{\mathbf{a}}^* - i\frac{231}{58}\widehat{\psi}_{\mathbf{f}}^*\widehat{\psi}_{\mathbf{b}}, \tag{33}$$

$$d_t\widehat{\psi}_{\mathbf{e}} + \left(5\mathrm{Re}^{-1} + \mathrm{Rh}^{-1}\right)\widehat{\psi}_{\mathbf{e}} = i\frac{19}{10}\widehat{\psi}_{\mathbf{f}}^*\widehat{\psi}_{\mathbf{a}} + i\frac{9}{10}\widehat{\psi}_{\mathbf{c}}^*\widehat{\psi}_{\mathbf{b}}^* + i\frac{99}{10}\widehat{\psi}_{\mathbf{f}}^*\widehat{\psi}_{\mathbf{b}} - i\frac{49}{10}\widehat{\psi}_{\mathbf{c}}\widehat{\psi}_{\mathbf{g}}^*, \tag{34}$$

$$d_t\widehat{\psi}_{\mathbf{f}} + \left(29\mathrm{Re}^{-1} + \mathrm{Rh}^{-1}\right)\widehat{\psi}_{\mathbf{f}} = i\frac{5}{58}\widehat{\psi}_{\mathbf{e}}^*\widehat{\psi}_{\mathbf{a}} + i\frac{231}{58}\widehat{\psi}_{\mathbf{d}}^*\widehat{\psi}_{\mathbf{b}} + i\frac{117}{58}\widehat{\psi}_{\mathbf{e}}^*\widehat{\psi}_{\mathbf{b}}. \tag{35}$$

The terms f_1, f_2 denote the forcing due to the first instability and contain the interaction terms with the modes presented in the previous section. At saturation the amplitudes of the modes $|\widehat{\psi}_{\mathbf{c}}|$, $|\widehat{\psi}_{\mathbf{d}}|$, $|\widehat{\psi}_{\mathbf{e}}|$, $|\widehat{\psi}_{\mathbf{f}}|$ scale like $(\mathrm{Rh} - \mathrm{Rh}_2^c)^{1/2}$. Next, we consider the triadic interaction between the modes $(\widehat{\psi}_{\mathbf{c}}, \widehat{\psi}_{\mathbf{e}}^*, \widehat{\psi}_{\mathbf{g}}^*)$ [see Fig. 6(c)]. In this triad, the mode $\widehat{\psi}_{\mathbf{g}}^* = \widehat{\psi}_{1,3}$ is excited by the nonlinear interaction between the two linearly excited modes $\widehat{\psi}_{\mathbf{c}} = \widehat{\psi}_{1,4}$ and $\widehat{\psi}_{\mathbf{e}}^* = \widehat{\psi}_{-2,1}$. The governing equation for $\widehat{\psi}_{\mathbf{g}}$

is given by

$$d_t\widehat{\psi}_{\mathbf{g}} + (10\mathrm{Re}^{-1} + \mathrm{Rh}^{-1})\widehat{\psi}_{\mathbf{g}} = i\frac{21}{5}\widehat{\psi}_{\mathbf{c}}\widehat{\psi}^*_{\mathbf{e}} + i\frac{4}{5}\widehat{\psi}_{\mathbf{h}}\widehat{\psi}^*_{\mathbf{c}}, \tag{36}$$

which at saturation gives rise to the scaling $|\widehat{\psi}_{\mathbf{g}}| \propto (\mathrm{Rh} - \mathrm{Rh}_2^c)$ for the amplitude. Then we consider the triad $(\widehat{\psi}^*_{\mathbf{c}}, \widehat{\psi}^*_{\mathbf{g}}, \widehat{\psi}_{\mathbf{h}})$, where the mode $\widehat{\psi}_{\mathbf{h}} = \widehat{\psi}_{0,1}$ is excited by the nonlinear interaction between the linearly excited mode $\widehat{\psi}^*_{\mathbf{c}} = \widehat{\psi}_{-1,4}$ and the nonlinearly excited mode $\widehat{\psi}^*_{\mathbf{g}} = \widehat{\psi}_{1,3}$ [see Fig. 6(d)]. The governing equation for $\widehat{\psi}_{\mathbf{h}}$ is given by

$$d_t\widehat{\psi}_{\mathbf{h}} + (\mathrm{Re}^{-1} + \mathrm{Rh}^{-1})\widehat{\psi}_{\mathbf{h}} = i\frac{7}{2}\big(\widehat{\psi}_{\mathbf{c}}\widehat{\psi}_{\mathbf{g}} - \widehat{\psi}^*_{\mathbf{c}}\widehat{\psi}^*_{\mathbf{g}}\big). \tag{37}$$

Thus, at saturation the mode scales like $|\widehat{\psi}_{\mathbf{h}}| = |\widehat{\psi}_{0,1}| \propto (\mathrm{Rh} - \mathrm{Rh}_2^c)^{3/2}$. To sum up, this reduced order model captures all the necessary scalings that were observed in the DNS for the second Hopf bifurcation.

V. CONCLUSION

We have studied the primary bifurcations of a forced Kolmogorov flow in a channel with free-slip boundary conditions in the lateral direction and periodic boundary conditions in the longitudinal direction, our aim being to mimic a parallel flow.

Unlike the doubly periodic Kolmogorov flow, where the first bifurcation is stationary, it can be a stationary or a Hopf bifurcation in the case of a laterally confined flow, depending on the value of the forcing wave number k_f. Stress-free lateral boundary conditions therefore change the qualitative behavior of the first bifurcation of the flow, as observed both in direct numerical simulations and by performing the linear stability analysis. In addition, when linear stability analysis predicts a stationary bifurcation (for $k_f \geqslant 4$), we discover a different behavior for k_f even for the full nonlinear problem. The nonlinearly saturated regime above the stationary bifurcation threshold is a traveling wave, where both the amplitude and the oscillation frequency of the growing mode vanish at threshold. As we move away from the threshold the amplitude scales with an exponent $1/2$ and the oscillation frequency with an exponent 1 of the distance to the threshold. This is related to an amplitude equation of this stationary bifurcation that involves a complex coefficient in the nonlinear term. We have understood why this behavior does not occur for k_f odd using a symmetry argument. Using a truncated model, we derived an amplitude equation with the required properties for $k_f = 4$. This reduced model displays the scaling observed in the DNS. We expect that stationary drift bifurcations can also occur in the case of other parallel flows.

A secondary instability occurs when $\mathrm{Rh} = \mathrm{Rh}_2^c$ and corresponds to a Hopf bifurcation. This leads to the generation of the largest scale mode in the system $\widehat{\psi}_{0,1}$, i.e., a large-scale shear flow with half a wave length in the spanwise direction and no dependence on the streamwise direction. Its amplitude displays a surprising scaling $(\mathrm{Rh} - \mathrm{Rh}_2^c)^{3/2}$. Using a truncated model, we find that the large-scale shear is not a bifurcating mode for $\mathrm{Rh} = \mathrm{Rh}_2^c$ but is nonlinearly excited by the bifurcating modes, which explains the observed scaling. It is surprising that these odd scaling laws at first sight are not reported more often in experiments where it is difficult to determine if the measured quantity is proportional to the amplitude of the bifurcating modes or to their harmonics.

ACKNOWLEDGMENTS

The authors would like to thank A. Alexakis, J. Chapman, P. Chossat, P. J. Ioannou, and T. Mullin for useful discussions. CEFIPRA is acknowledged for support with project 6104-1. K.S. acknowledges National Supercomputing Mission (NSM) for providing computing resources of PARAM Shakti at IIT Kharagpur, which is implemented by C-DAC and supported by the Ministry of Electronics and Information Technology (MeitY) and Department of Science and Technology (DST), Government of India.

APPENDIX: DERIVATION OF THE AMPLITUDE EQUATIONS

Here we provide details for the derivation of the amplitude equations (25) and (26) starting from the governing equations (18)–(21). We start with the linearized equations (22) and (23) written in the matrix form, $d_t\boldsymbol{\Psi} = \mathcal{A}\boldsymbol{\Psi}$:

$$d_t\begin{bmatrix}\widehat{\psi}_{\mathbf{p}}\\ \widehat{\psi}^*_{\mathbf{q}}\end{bmatrix} = \begin{bmatrix}-(10\mathrm{Re}^{-1}+\mathrm{Rh}^{-1}) & i\frac{12}{10}\psi_0\\ -i2\psi_0 & -\left(18\mathrm{Re}^{-1}+\mathrm{Rh}^{-1}\right)\end{bmatrix}\begin{bmatrix}\widehat{\psi}_{\mathbf{p}}\\ \widehat{\psi}^*_{\mathbf{q}}\end{bmatrix}. \tag{A1}$$

The solution to $\det(\mathcal{A}-\lambda\mathcal{I})=0$ gives the following two eigenvalues:

$$\lambda_1 = -\frac{2\sqrt{20\mathrm{Re}^{-2}(\mathrm{Rh}^{-1}+16\mathrm{Re}^{-1})^2+3}}{\sqrt{5}(\mathrm{Rh}^{-1}+16\mathrm{Re}^{-1})} - \mathrm{Rh}^{-1} - 14\mathrm{Re}^{-1}, \tag{A2}$$

$$\lambda_2 = \frac{2\sqrt{20\mathrm{Re}^{-2}(\mathrm{Rh}^{-1}+16\mathrm{Re}^{-1})^2+3}}{\sqrt{5}(\mathrm{Rh}^{-1}+16\mathrm{Re}^{-1})} - \mathrm{Rh}^{-1} - 14\mathrm{Re}^{-1}. \tag{A3}$$

We see that the eigenvalue λ_1 is always negative, and the threshold of the instability is found by putting $\lambda_2 = 0$, which gives the threshold $\mathrm{Rh}_c^{-1} \approx 1.229$ for $\mathrm{Re} = 1000$. The associated eigenvectors denoted as $\mathbf{V}_1$, $\mathbf{V}_2$ are given by

$$\mathbf{V_1} = \begin{bmatrix}-\frac{1}{5}i\left(\sqrt{5}\sqrt{20\mathrm{Rh}^{-2}\mathrm{Re}^{-2}+640\mathrm{Rh}^{-1}\mathrm{Re}^{-3}+5120\mathrm{Re}^{-4}+3}-10\mathrm{Rh}^{-1}\mathrm{Re}^{-1}-160\mathrm{Re}^{-2}\right)\\ 1\end{bmatrix}, \tag{A4}$$

$$\mathbf{V_2} = \begin{bmatrix}\frac{1}{5}i\left(\sqrt{5}\sqrt{20\mathrm{Rh}^{-2}\mathrm{Re}^{-2}+640\mathrm{Rh}^{-1}\mathrm{Re}^{-3}+5120\mathrm{Re}^{-4}+3}+10\mathrm{Rh}^{-1}\mathrm{Re}^{-1}+160\mathrm{Re}^{-2}\right)\\ 1\end{bmatrix}. \tag{A5}$$

We then express the variables $\boldsymbol{\Psi}(t)$ as a linear combination of the two eigenvectors with amplitudes $P_1(t)$, $P_2(t)$,

$$\boldsymbol{\Psi}(t) = P_1(t)\mathbf{V}_1 + P_2(t)\mathbf{V}_2 = \mathcal{V}\mathbf{P}, \tag{A6}$$

where $\mathcal{V} = [\mathbf{V}_1\ \mathbf{V}_2]$ denotes the eigenvector matrix and $\mathbf{P} = [{}^{P_1}_{P_2}]$ denotes the amplitude vector.

To get the nonlinear system of equations in terms of the eigenvectors, we start with

$$\begin{aligned} d_t\boldsymbol{\Psi} &= \mathcal{A}\boldsymbol{\Psi} + \begin{bmatrix}-i\frac{6}{5}\widetilde{\psi}_{\mathbf{k}}\widehat{\psi}^*_{\mathbf{q}} - i\frac{21}{5}\widehat{\psi}_{\mathbf{r}}\widehat{\psi}^*_{\mathbf{q}} - i\frac{18}{5}\widehat{\psi}_{\mathbf{p}}\widehat{\psi}_{\mathbf{r}}\\ -2i\widetilde{\psi}_{\mathbf{k}}\widehat{\psi}^*_{\mathbf{p}} + i\widehat{\psi}_{\mathbf{r}}\widehat{\psi}^*_{\mathbf{p}}\end{bmatrix}\\ &= \mathcal{A}\boldsymbol{\Psi} + \mathbf{N}, \end{aligned} \tag{A7}$$

where $\mathbf{N}$ denotes the nonlinear terms and $\widetilde{\psi}_{\mathbf{k}}$ denotes the deviation of $\widehat{\psi}_{\mathbf{k}}$ from the base flow ψ_0 due to the nonlinearity, namely, $\widehat{\psi}_{\mathbf{k}} = \psi_0 - \widetilde{\psi}_{\mathbf{k}}$. Doing the eigendecomposition of the matrix $\mathcal{A}$, we get

$$d_t\boldsymbol{\Psi} = \mathcal{V}\mathcal{D}\mathcal{V}^{-1}\boldsymbol{\Psi} + \mathbf{N}, \tag{A8}$$

where $\mathcal{D}$ is a diagonal matrix whose diagonal entries are the eigenvalues λ_1 and λ_2. Taking $\mathcal{V}^{-1}$ on both sides leads to the equation

$$d_t\left(\mathcal{V}^{-1}\boldsymbol{\Psi}\right) = \mathcal{D}\left(\mathcal{V}^{-1}\boldsymbol{\Psi}\right) + \mathcal{V}^{-1}\mathbf{N}. \tag{A9}$$

From (A6) we can write $\mathcal{V}^{-1}\boldsymbol{\Psi} = \mathbf{P}$, which gives

$$d_t\mathbf{P} = \mathcal{D}\mathbf{P} + \mathcal{V}^{-1}\mathbf{N}. \tag{A10}$$

Since $\lambda_1 < 0$ and the nonlinear terms do not force $P_1(t)$, the amplitude $|P_1|$ goes to zero in the long time limit, implying that we can express $\widehat{\psi}_{\mathbf{p}}$, $\widehat{\psi}_{\mathbf{q}}$ in terms of $P_2(t)$ only. The nonlinear vector $\mathbf{N}$

involves terms with $\widetilde{\psi}_{\mathbf{k}}$ that is nonzero above the first instability threshold and is modified by terms involving $\widehat{\psi}_{\mathbf{p}}$, $\widehat{\psi}_{\mathbf{q}}$ [see Eq. (18)]. The $\mathbf{N}$ vector also involves $\widehat{\psi}_{\mathbf{r}}$, which is excited by terms involving $\widehat{\psi}_{\mathbf{p}}$, $\widehat{\psi}_{\mathbf{q}}$ [see Eq. (21)]. The nonlinear term needed to find $\widetilde{\psi}_{\mathbf{k}}$, and $\widehat{\psi}_{\mathbf{r}}$ is given by the expression $\widehat{\psi}^*_{\mathbf{p}}\widehat{\psi}^*_{\mathbf{q}} - \widehat{\psi}_{\mathbf{p}}\widehat{\psi}_{\mathbf{q}}$ [see Eqs. (18) and (21)]. This can be written in terms of $P_2(t)$ as

$$\widehat{\psi}^*_{\mathbf{p}}\widehat{\psi}^*_{\mathbf{q}} - \widehat{\psi}_{\mathbf{p}}\widehat{\psi}_{\mathbf{q}} \to -2i\zeta_2|P_2|^2, \tag{A11}$$

where ζ_2 is given by

$$\zeta_2 = \tfrac{1}{5}(\sqrt{5}\sqrt{20\mathrm{Rh}^{-2}\mathrm{Re}^{-2} + 640\mathrm{Rh}^{-1}\mathrm{Re}^{-3} + 5120\mathrm{Re}^{-4} + 3} + 10\mathrm{Rh}^{-1}\mathrm{Re}^{-1} + 160\mathrm{Re}^{-2}). \tag{A12}$$

Here $P_2(t)$ is an oscillating complex quantity for the four-mode model or is a stationary real quantity for the three-mode model and in both cases $|P_2|$ is independent of time. This gives the following expressions for $\widetilde{\psi}_{\mathbf{k}}$ and $\widehat{\psi}_{\mathbf{r}}$:

$$\widetilde{\psi}_{\mathbf{k}} = \frac{6}{16\mathrm{Re}^{-1} + \mathrm{Rh}^{-1}}\zeta_2|P_2|^2, \tag{A13}$$

$$\widehat{\psi}_{\mathbf{r}} = \frac{12}{4\mathrm{Re}^{-1} + \mathrm{Rh}^{-1}}\zeta_2|P_2|^2. \tag{A14}$$

Now we need the expression of $\mathcal{V}^{-1}$ to solve Eq. (A10), its matrix form is denoted as

$$\mathcal{V}^{-1} = [\mathbf{V}_1\ \mathbf{V}_2]^{-1} = \begin{bmatrix} \beta_1 & \beta_2 \\ -\beta_1 & \beta_3 \end{bmatrix}, \tag{A15}$$

where β_1, β_2, β_3 are defined as

$$\beta_1 = \frac{i\sqrt{5}}{2\sqrt{20\mathrm{Rh}^{-2}\mathrm{Re}^{-2} + 640\mathrm{Rh}^{-1}\mathrm{Re}^{-3} + 5120\mathrm{Re}^{-4} + 3}}, \tag{A16}$$

$$\beta_2 = \frac{\sqrt{5}\sqrt{20\mathrm{Rh}^{-2}\mathrm{Re}^{-2} + 640\mathrm{Rh}^{-1}\mathrm{Re}^{-3} + 5120\mathrm{Re}^{-4} + 3} + 10\mathrm{Rh}^{-1}\mathrm{Re}^{-1} + 160\mathrm{Re}^{-2}}{2\sqrt{5}\sqrt{20\mathrm{Rh}^{-2}\mathrm{Re}^{-2} + 640\mathrm{Rh}^{-1}\mathrm{Re}^{-3} + 5120\mathrm{Re}^{-4} + 3}}, \tag{A17}$$

$$\beta_3 = \frac{\sqrt{5}\sqrt{20\mathrm{Rh}^{-2}\mathrm{Re}^{-2} + 640\mathrm{Rh}^{-1}\mathrm{Re}^{-3} + 5120\mathrm{Re}^{-4} + 3} - 10\mathrm{Rh}^{-1}\mathrm{Re}^{-1} - 160\mathrm{Re}^{-2}}{2\sqrt{5}\sqrt{20\mathrm{Rh}^{-2}\mathrm{Re}^{-2} + 640\mathrm{Rh}^{-1}\mathrm{Re}^{-3} + 5120\mathrm{Re}^{-4} + 3}}. \tag{A18}$$

Substituting the expressions for $\widetilde{\psi}_{\mathbf{k}}$, $\widehat{\psi}_{\mathbf{r}}$ from Eqs. (A13) and (A14) and the expression of $\mathcal{V}^{-1}$ from Eq. (A15), into the Eq. (A10) gives the amplitude equations for the growing eigenmode $P_2(t)$. By setting $\widehat{\psi}_{\mathbf{r}} = 0$ in the nonlinear term N of Eq. (A10) we get the amplitude equation for the stationary bifurcation [see Eq. (25)]. By considering all four modes, with $\widehat{\psi}_{\mathbf{r}}$ taken from Eq. (A14), the resulting amplitude equation is given by Eq. (26) which leads to oscillations.

[1] V. I. Arnold and L. D. Meshalkin, Seminar led by A. N. Kolmogorov on selected problems of analysis (1958–1959), Usp. Mat. Nauk **15**, 247 (1960).

[2] L. Meshalkin and Y. Sinai, Investigation of the stability of a stationary solution of a system of equations for the plane movement of an incompressible viscous liquid, J. Appl. Math. Mech. **25**, 1700 (1961).

[3] A. A. Nepomniashchii, On stability of secondary flows of a viscous fluid in unbounded space, Prikl. Mat. Mekh. **40**, 886 (1976).

[4] G. I. Sivashinsky, Weak turbulence in periodic flows, Physica D **17**, 243 (1985).

[5] D. Lucas and R. R. Kerswell, Spatiotemporal dynamics in two-dimensional Kolmogorov flow over large domains, J. Fluid Mech. **750**, 518 (2014).

[6] N. F. Bondarenko, M. Z. Gak, and F. V. Dolzhanskii, Laboratory and theoretical models of plane periodic flow, Izv. Akad. Nauk (Fiz. Atmosfer. Okeana) **15**, 1017 (1979).
[7] J. Sommeria, Experimental study of the two-dimensional inverse energy cascade in a square box, J. Fluid Mech. **170**, 139 (1986).
[8] J. M. Burgess, C. Bizon, W. D. McCormick, J. B. Swift, and H. L. Swinney, Instability of the Kolmogorov flow in a soap film, Phys. Rev. E **60**, 715 (1999).
[9] A. Thess, Instabilities in two-dimensional spatially periodic flows. Part I: Kolmogorov flow, Phys. Fluids A **4**, 1385 (1992).
[10] H. Fukuta and Y. Murakami, Side-wall effect on the long-wave instability in Kolmogorov flow, J. Phys. Soc. Jpn. **67**, 1597 (1998).
[11] Y. B. Kolesnikov, Investigation of a shear flow instability in a magnetic field, Magn. Gidrodin. **1**, 60 (1985).
[12] A. M. Batchaev and V. M. Ponomarev, Experimental and theoretical investigation of Kolmogorov flow on a cylindrical surface, Fluid Dyn. **24**, 675 (1989).
[13] Z.-M. Chen and W. G. Price, Supercritical regimes of liquid-metal fluid motions in electromagnetic fields: Wall-bounded flows, Proc. R. Soc. A **458**, 2735 (2002).
[14] Z.-M. Chen and W. G. Price, Secondary fluid flows driven electromagnetically in a two-dimensional extended duct, Proc. R. Soc. A **461**, 1659 (2005).
[15] Z.-M. Chen, Instability of the Kolmogorov flow in a wall-bounded domain, J. Phys. Commun. **4**, 015001 (2020).
[16] J. Guckenheimer and P. Holmes, *Nonlinear Oscillations, Dynamical Systems and Bifurcations of Vector Fields*, Applied Mathematical Science (Springer Verlag, New York, 1983), Vol. 42.
[17] P. Tabeling, B. Perrin, and S. Fauve, Instability of a linear array of forced vortices, Europhys. Lett. **3**, 459 (1987).
[18] P. N. Guzdar, J. M. Finn, A. V. Rogalsky, and J. F. Drake, Two-dimensional nonlinear dynamics of four driven vortices, Phys. Rev. E **49**, 2062 (1994).
[19] F. Pétrélis, S. Aumaître, and S. Fauve, Effect of Phase Noise on Parametric Instabilities, Phys. Rev. Lett. **94**, 070603 (2005).
[20] V. Dallas, K. Seshasayanan, and S. Fauve, Bifurcations between turbulent states in a two-dimensional shear flow, Phys. Rev. Fluids **5**, 084610 (2020).
[21] D. Gottlieb and S. A. Orszag, *Numerical Analysis of Spectral Methods: Theory and Applications*, CBMS-NSF Regional Conference Series in Applied Mathematics, Vol. 26 (SIAM, Philadelphia, 1977).
[22] D. O. Gómez, P. D. Mininni, and P. Dmitruk, Parallel simulations in turbulent MHD, Phys. Scr. **2005**, 123 (2005).
[23] P. Hirschberg and E. Knobloch, Mode interactions in large aspect ratio convection, J. Nonlinear Sci. **7**, 537 (1997).
[24] M. Gorman, H. L. Swinney, and D. A. Rand, Doubly Periodic Circular Couette Flow: Experiments Compared with Predictions from Dynamics and Symmetry, Phys. Rev. Lett. **46**, 992 (1981).
[25] D. Rand, Dynamics and symmetry. Predictions for modulated waves in rotating fluids, Arch. Ration. Mech. Anal. **79**, 1 (1982).
[26] D. Armbruster, B. Nicolaenko, N. Smaoui, and P. Chossat, Analyzing bifurcations in the Kolmogorov flow equations, in *Dynamics, Bifurcation and Symmetry*, edited by P. Chossat (Kluwer Academic Publishers, Netherlands, 1994), pp. 11–33.
[27] I. Bosch Vivancos, P. Chossat, and I. Melbourne, New planforms in systems of partial differential equations with Euclidean symmetry, Arch. Rational Mech. Anal. **131**, 199 (1995).
[28] J. D. Crawford, M. Golubitsky, M. G. M. Gomes, E. Knobloch, and I. N. Stewart, Boundary conditions as symmetry constraints, in *Singularity Theory and Its Applications*, edited by R. M. Robert and I. N. Stewart (Springer-Verlag, Heidelberg, 1991), pp. 63–79.
[29] I. Melbourne, Hidden symmetries on partially unbounded domains, Physica D **143**, 226 (2000).
[30] S. Fauve, Pattern forming instabilities, in *Hydrodynamics and Nonlinear Instabilities*, edited by C. Godrèche and P. Manneville (Cambridge University Press, Cambridge, 1998), pp. 387–492.